Recent advances in using Chinese Earth observation satellites for remote sensing of vegetation

Zhengyang Zhang[1], Lei Lu[1], Yuhe Zhao[1], Yuanyuan Wang[2], Xuanlong Ma[1,*]

[1] College of Earth and Environmental Sciences, Lanzhou University, Lanzhou, Gansu, 730000 China

[2] National Satellite Meteorological Centre (NSMC), Beijing, 100082 China

* correspondence to: X.M. (xlma@lzu.edu.cn)

Abstract

Vegetation is an important component of terrestrial ecosystem as it supports other biological activities through the photosynthetic production. The biophysical and biochemical parameters of vegetation retrieved from satellite observations have been used extensively in studying the physiological states and growing conditions of vegetation that enabling global vegetation monitoring. Most of vegetation remote sensing applications using data from MODIS, Landsat, and Sentinel, though it would be beneficial, from the user perspective, to have an even more diverse data sources that not only secure data sustainability in case satellite retirement or sensor failure, but also enables research opportunities such as multi-sensor data fusion/integration and multi-angle remote sensing that can take advantage of observations acquired from different spaceborne sensors. In this regard, it would be worth to explore the potential of the large number of Chinese Earth Observation Satellites (CEOS) that have been put into orbit over past decade. Here we summarized the recent advances in applying CEOS remote sensing of vegetation and its associated applications. We focused on the uncertainty and limitations for retrieving several commonly-used vegetation parameters by critically examining the case studies conducted over different vegetation types. Suggestions for research opportunities that can benefit from the additional data from CEOS are also provided. The hope is to provide the community an overview of what could be useful to their specific ecological, environmental and global change studies by leveraging the growing data volume from the orbiting CEOS sensors.

Keywords: remote sensing of vegetation, biophysical and biochemical variables, global change, multi-sensor fusion, data continuity

1 Introduction

Vegetation remote sensing refers to the retrieval of biochemical and biophysical parameters of vegetation using satellite observations (Aplin 2005). Commonly used vegetation parameters include vegetation indices (VI), leaf area index (LAI), fractional vegetation cover (FVC) and aboveground biomass (AGB) (Cohen and Goward 2004; Kerr and Ostrovsky 2003; Wulder et al. 2004). These parameters have been widely used as diagnostic proxy as well as input to prediction models in the field of agriculture, ecology, environmental science, and global change (Gianelle et al. 2009; Nara and Sawada 2021; Pettorelli et al. 2005)

Over past few decades, the field of remote sensing of vegetation is witnessing rapid advances not only in retrieval algorithms, but also in its associated applications. Like many other natural sciences, instrument plays a fundamental role. As such, a large credit of the success of vegetation remote sensing should be given to the enormous amount of investment and efforts to launch and maintain the orbiting satellites, which is usually done by state government. Spaceborne sensors such as AVHRR

(Advanced Very-High-Resolution Radiometer), MODIS (Moderate-resolution Imaging Spectroradiometer) and ETM (Enhanced Thematic Mapper), have acquired huge amount of science-quality data that led to a surge of applications in vegetation remote sensing field(Davis et al. 2017; Liu et al. 2018; Mancino et al. 2020; Zhang et al. 2017; Zhou et al. 2018; Zoungrana et al. 2018)

Over past decade, China has launched more than a dozen of Earth Observation satellites that carry instruments ranging from multispectral, hyperspectral, to Synthetic Aperture Rader (SAR), in together we termed as Chinese Earth Observation Satellites (CEOSs) (Figure 1). There have been many studies that used data from CEOSs for retrieving vegetation parameters, while a systemic review on the potentials and limitations of sensors onboard CEOSs for remote sensing of vegetation is not yet available. Questions such as to what extent the sensor specifications resemble the industry-standard sensors such as MODIS or ETM/OLI, what are the retrieval accuracies for commonly-used vegetation parameters in different ecosystem types, and what kind of multi-sensor research opportunities are enabled by adding CEOSs to other commonly-used satellites? It would be good for the community to know these so that the end-users can better leverage the significant amount of investment on the CEOSs. This review is dedicated to answer above questions. To make this review reaching a broader community, most of the literatures we reviewed in English and published in well-known journals, with the remaining published in Chinese journals with English abstract. In addition, the English weblink to the data portals of CEOSs are also provided.

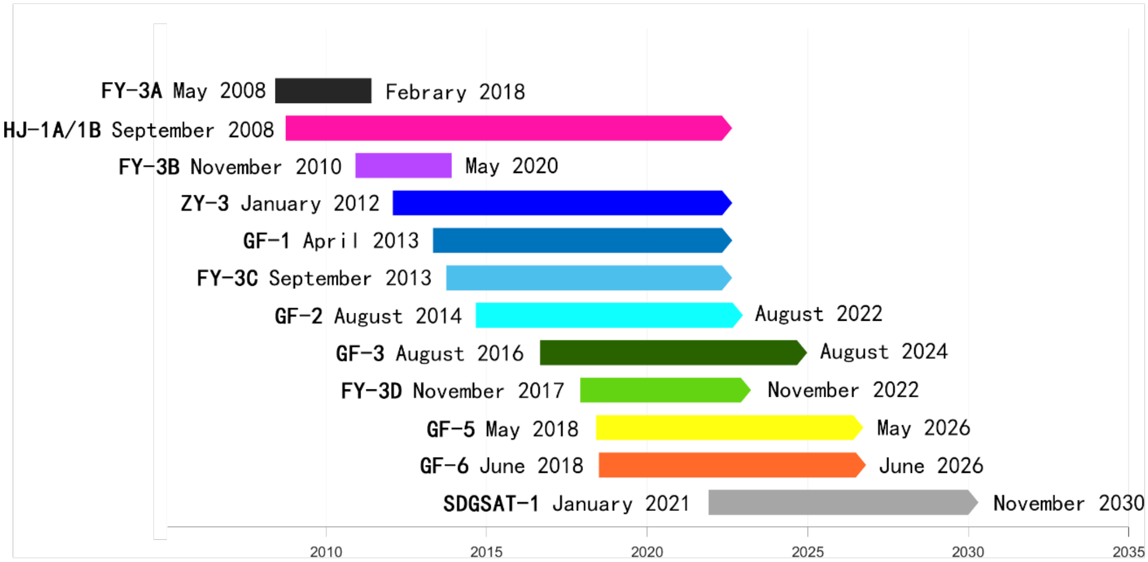

Figure 1 Timelines of several major CEOSs (FY: FengYun Meteorological Satellite; GF: GaoFen Satellite; ZY: ZiYuan Satellite; HJ: HuanJing satellite; SDGSAT: Sustainable Development Goals Satellite)

2 Overview of the CEOS sensor specifications

At present, the four major constellations of CEOS that can be used for land vegetation remote sensing include HJ (HuanJing, or literally in Chinese means "Environment"), GF (GaoFen, or "High-resolution"), FY (FengYun, or "Wind and Cloud") and ZY (ZiYuan, or "Resources"). Sensors onboard these satellites represent a wide range of spatial resolution from coarse (lower than 30 m), medium (20 – 30 m), to high (higher than 20 m). Instruments are also very diverse, ranging from panchromatic, visible, multispectral, hyperspectral to Synthetic Aperture Radar (SAR). Table 1 provides a comprehensive summary of the CEOS sensor specifications and Figure 2 presents the comparison in spectral band configurations between the CEOS optical sensors and the sensors from other space agencies.

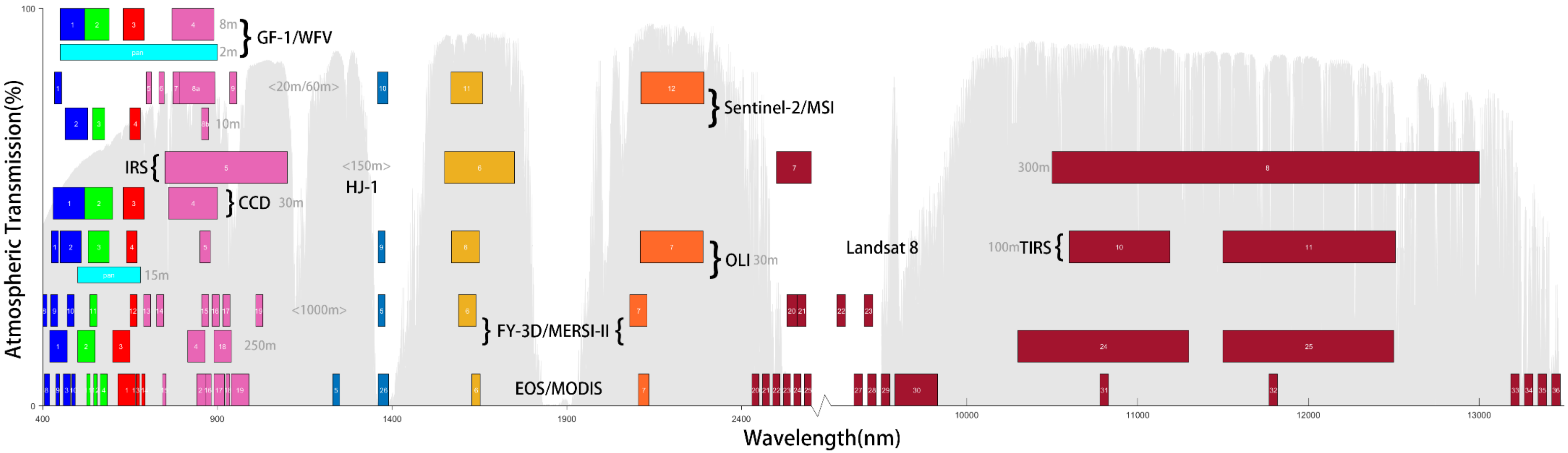

Figure 2 Spectral band comparison between sensors onboard CEOSs and satellites from other space agencies. (each bar represents a single band and the width of the bar indicates bandwidth. The number on the bar indicates the band number. Spatial resolution of each band is also indicated with grey-colour text. The background shows the atmospheric transmittance at the standard atmosphere configuration.)

2.1 GaoFen Satellites

GaoFen (GF) is a series of Chinese high-resolution Earth imaging satellite for the state-sponsored program Chine High-resolution Earth Observation System (CHEOS). The firs of the GF series satellites, GaoFen-1 (GF-1) was launched on April 26, 2013, with a designing life of 5-8 years. It carries a Wide-Field View multispectral sensors (WFV) with 16 m resolution, a Panchromatic / Multispectral sensors (PMS) with 2 m spatial resolution in panchromatic mode and 8 m spatial resolution in multispectral mode. So far there have been four nearly identical GF-1 launched into orbit. GaoFen-6 (GF-6) is another multispectral satellite launched on June 2, 2018, with a design life of 8 years. Equipped with the WFV and PMS sensor as GF-1, GF-6 also adds a "red edge" band to reflect the unique spectral characteristics of crops. GF-1/6 WFV and PMS sensors are similar to Sentinel-2/MSI and SPOT-6(7)/NAOMI, respectively (Appendix Table A1 and A2).

GaoFen-2 (GF-2) is a high spatial resolution satellite, launched on August 19, 2014, with a designing life of 5-8 years. GF-2 carries a PMS which has a higher spatial resolution than that on GF-1/6, with a ground resolution of 0.8 m in panchromatic mode and 3.2 m in multispectral mode (Huang et al. 2018; Pan 2015). GF-2/PMS is similar to QuickBird and WorldView satellites (Appendix Table A3).

GaoFen-3 (GF-3) is a SAR constellation consists of two satellites, GF-3 01 and GF-3 02, launched in August 9, 2016 and November 22, 2021, respectively. Both satellites carry the C-band multi-polarization SAR with a spatial resolution range from 1 m-500 m. GF-3 is very similar to ESA's Sentinel-1 (Appendix Table A4).

GaoFen-4 (GF-4) is a geostationary orbiting satellite that was launched on December 29, 2015 with a design life of 8 years. GF-4/PMS has 5 channels located between visible and near-infrared spectrum with a spatial resolution of 50 m, and 1 channel in mid-infrared spectrum with a spatial resolution of 400 m. GF-4/PMS is similar to GOES-R/ABI and Himawari-8/AHI.

GaoFen-5 (GF-5) is a full-spectrum hyperspectral satellite launched on May 9, 2018, with a design life of 8 years. GF-5 carries the Advanced Hyperspectral Imager (AHSI) that has 30 m spatial resolution and 330 bands from 400 – 2500 nm. GF-5/AHSI is similar to EO-1/Hyperion and DLR/DESIS(Appendix Table A5).

Table 1 Chinese GaoFen satellites parameters

Satellite	Load	Band No.	Spectral Range (μm)	Spatial Resolution (m)	Swath Width (km)	Revisit Cycle (days)	Similar Sensors
GF-1	Panchromatic & Multispectral Camera (PMS)	pan	0.45~0.90	2	60 (2 Cameras)	4	SPOT-6(7)/ NAOMI
		1	0.45~0.52	8			
		2	0.52~0.59				
		3	0.63~0.69				
		4	0.77~0.89				
	Wide-Field View Multispectral Camera (WFV)	5	0.45~0.52	16	800 (4 Cameras)	2	Sentinel-2/ MSI
		6	0.52~0.59				
		7	0.63~0.69				
		8	0.77~0.89				
GF-2	PMS	pan	0.45~0.90	1	45 (2 Cameras)	5	WorldView-3/ WV110
		1	0.45~0.52	4			
		2	0.52~0.59				
		3	0.63~0.69				
		4	0.77~0.89				
GF-3	Synthetic Aperture Radar (SAR)	-	C-band: 4-8 GHz	1-500	5-650	Single Vision: <3d; Double	Sentinel-1

						Vision: <1.5d	
GF-4	PMS	pan	0.45~0.90	50	500	20 Seconds	
		1	0.45~0.52				
		2	0.52~0.60				
		3	0.63~0.69				
		4	0.76~0.90				
	Infrared Multispectral Camera(IRS)	5	3.50~4.10	400	400		
GF-5	Advanced Hyperspectral Imager(AHSI)	1-300	0.40~2.50	-	60	5	DLR & PRISMA
	Visible and Infrared Multispectral Imager(VIMI)	1	0.45~0.52	20			Sentinel-2/ MSI
		2	0.52~0.60				
		3	0.62~0.68				
		4	0.76~0.86				
		5	1.55~1.75				
		6	2.08~2.35				
		7	3.50~3.90	40			
		8	4.85~5.05				
		9	8.01~8.39				
		10	8.42~8.83				
		11	10.3~11.3				
		12	11.4~12.5				
GF-6	PMS	Same as GF-1/PMS			90 (2 Cameras)	4	Same as GF-1
	WFV	1	0.45~0.52	16	800 (4 Cameras)	2	
		2	0.52~0.59				
		3	0.63~0.69				
		4	0.77~0.89				
		5	0.69~0.73				
		6	0.73~0.77				
		7	0.40~0.45				
		8	0.59~0.63				

105 ***2.2 ZiYuan-3 satellites***

ZiYuan-3 (ZY-3) is Chinese first civilian high-resolution optical stereo mapping satellite (Li 2012; Tang and Hu 2018; Wang et al. 2014a). ZY-3 01 and 02 satellites were launched on January 9, 2012 and May 30, 2016, respectively, forming a constellation with a design life of 5 years. ZY-3 carries a forward-looking panchromatic TDI (Time Delayed and Integration) CCD camera with a resolution of 2.1 m, two forward-looking and backward-looking panchromatic TDI CCD cameras with a resolution of 3.5 m, and a forward-looking multispectral camera with a resolution of 5.8 m. ZY-3 can achieve seamless image coverage within 84° of the Earth's north and south latitudes by side-swinging, and can achieve global image coverage every 59 days, providing long-term, continuous, stable and rapid acquisition of 2.1 m resolution stereo images and 6 m multispectral images of the world. ZY-3 also carries a multispectral camera (MUX) which is similar to GF-1/PMS.

Table 2 Chinese ZiYuan-3 satellites parameters

Satellite	Load		Band No.	Spectral Range (μm)	Spatial Resolution (m)	Swath Width (km)	Revisit Cycle (days)	Similar Sensors
ZY-3 (01/02)	CCD	Forward	1	0.50~0.80	3.5	52	5	SPOT-6(7)/ NAOMI
		Backward						
		Nadir			2.1	51		
	Multispectral Camera (MUX)		1	0.45~0.52	6	51	3-5	
			2	0.52~0.59				
			3	0.63~0.69				
			4	0.77~0.89				

2.3 HuanJing-1 satellites

HJ-1 satellites are small Chinese EO satellites operated by the China Centre for Resources Satellite Data and Application (CRESDA) that is aiming to provide all-weather imagery. HJ-1 consists of two optical satellite 1A and 1B, and one radar satellite, 1C. HJ-1A and 1B were lunched on September 6, 2008 and carried a 30 m resolution CCD camera and a 100 m resolution hyperspectral Imager (HSI), while the HJ-1B satellite carries a 30 m resolution CCD camera and a 150 m resolution Infrared Scanner (IRS). The HJ-1 satellite have a design life of 3 years and are still functioning in orbit. HJ-1/ HSI and IRS are similar to EO-1/Hyperion and Landsat-8/TIRS, respectively.

Table 3 Chinese HuanJing-1 satellites parameters

Satellite	Load	Band No.	Spectral Range (μm)	Spatial Resolution (m)	Swath Width (km)	Revisit Cycle (days)	Similar Sensors
HJ-1A	CCD	1	0.43~0.52	30	360(Single) 700(Parallel)	4	Landsat satellites
		2	0.52~0.60				
		3	0.63~0.69				
		4	0.76~0.9				
	Hyperspectral Imager (HSI)	-	0.45~0.95 (110-128 bands)	100	50	4	
HJ-1B	CCD	1	0.43~0.52	30	360(Single) 700(Parallel)	4	
		2	0.52~0.60				
		3	0.63~0.69				
		4	0.76~0.90				
	Infrared Scanner (IRS)	5	0.75~1.10	150	720	4	
		6	1.55~1.75				
		7	3.50~3.90				
		8	10.5~12.5	300			

2.4 FengYun-3 Satellites

FengYun-3 (FY-3) are new generation of Chinese polar-orbiting meteorological satellites. FY-3A and FY-3B, launched on May 27, 2008 and November 5, 2011respectively, are the first two that carry a Visible and Infra-Red Radiometer (VIRR) and a Medium Resolution Spectral Imager (MERSI), among with other sensors for atmospheric sensing (Dong et al. 2009; Zhang et al. 2015). FY-3C and FY-3D, launched on September 23, 2013 and November 15, 2017 respectively, carry an upgraded second generation MERSI instrument (MERSI-II) (Wang et al. 2019). MERSI-II has a better ability on the infrared information detection than MERSI with the wide spectral channel expanded to six mid- and far-infrared channels. Except that, MERSI-II also adds the shortwave infrared channel (1.38μm) and the onboard calibrate instrument for the cirrus detection and calibration. FY-3/VIRR is similar to NOAA/AVHRR while MERSI is very similar to EOS/MODIS.

GF, ZY, HJ satellites data are available at China Centre For Resources Satellite Data and Application (http://www.cresda.com/EN/), while FY data are available at National Satellite Meteorological Center (http://www.nsmc.org.cn/nsmc/en/home/index.html). All data access platforms are featured with English language support. In the following section we review the recent applications of using above sensors for retrieving vegetation parameters.

Table 3 Chinese FengYun-3 satellites parameters

Satellite	Load	Band No.	Spectral Range (μm)	Spatial Resolution (m)	Swath Width (km)	Revisit Cycle (days)	Similar Sensors
FY-3C	Visible and Infra-Red Radiometer (VIRR)	1	0.58-0.68	1000	2800	5.5	
		2	0.84-0.89				
		3	3.55-3.93				
		4	10.3-11.3				
		5	11.5-12.5				
		6	1.55-1.64				
		7	0.43-0.48				
		8	0.48-0.53				
		9	0.53-0.58				
		10	1.325-1.395				
	Medium Resolution Spectral Imager (MERSI)	1	0.42~0.52	250	2800	5.5	MODIS、MERIS
		2	0.5~0.6				
		3	0.6~0.7				
		4	0.815~0.915				
		5	8.75~13.75				
		6	0.392~0.432	1000			
		7	0.423~0.463				
		8	0.47~0.51				
		9	0.5~0.54				
		10	0.545~0.585				
		11	0.63~0.67				
		12	0.665~0.705				
		13	0.745~0.785				
		14	0.845~0.885				
		15	0.885~0.925				
		16	0.92~0.96				
		17	0.96~1				
		18	1.01~1.05				
		19	1.59~1.69				
		20	2.08~2.18				
FY-3D	Medium Resolution Spectral Imager-Ⅱ (MERSI-Ⅱ)	1	0.402~0.422	1000	2800	5.5	MODIS、MERIS
		2	0.433~0.453				
		3	0.445~0.495	250			
		4	0.48~0.5	1000			
		5	0.525~0.575	250			
		6	0.545~0.565	1000			
		7	0.625~0.675	250			

	8	0.66~0.68	1000
	9	0.699~0.719	
	10	0.736~0.756	
	11	0.855~0.875	
	12	0.84~0.89	250
	13	0.895~0.915	1000
	14	0.926~0.946	
	15	0.915~0.965	
	16	1.23~1.31	
	17	1.365~1.395	
	18	1.615~1.665	
	19	2.105~2.155	
	20	2.99~3.17	
	21	3.9725~4.1275	
	22	6.95~7.45	
	23	8.4~8.7	
	24	10.3~11.3	250
	25	11.5~12.5	

3 Vegetation parameters retrievals using CEOS sensors

3.1 Vegetation Index

Vegetation indices (VIs) such as normalized difference vegetation index (NDVI) are simple and effective parameter used to characterize vegetation cover and growth (Bannari et al. 1995; Kalaitzidis et al. 2010; Pettorelli 2013). With a spatial resolution as high as 16 m, VIs derived from GF-1/WFV provided enough spatial details for mapping vegetation in heterogeneous landscape (Zhao et al. 2019, 2020).Zhao et al. (Zhao et al. 2013) and Yuan et al. (Yuan et al. 2015) analyzed the relationships of several commonly used vegetation indices (i.e. NDVI, SAVI, and EVI) derived from HJ-1/CCD and Landsat-5/TM or Landsat-7/ETM+ and found that there was a significant positive correlation for all indices derived HJ or Landsat ($R^2 > 0.90$). Specifically, HJ-1/CCD NDVI is higher than Landsat NDVI in areas with sparse vegetation cover, while the opposite is true in areas with high vegetation cover, which can be attributed to the fact that the upper limit of the spectral range in the red band and the lower limit of the spectral range in the NIR band of HJ-1/CCD were entered in the range of 0.70~0.75 μm, which generally has smaller reflectance than the SRF of red and NIR band not cross the range used by, leading to smaller HJ-1/CCD NDVI values. Due to the spectral band similarity, Chen et al. (2015) was able to establish translation equations between HJ-1/CCD NDVI and EOS/MODIS NDVI, offering the potential for multi-sensor data fusion.

Wu et al. (2011) analyzed the relationship between FY-3A/MERSI and Terra/MODIS VIs and further verified them using ground VI measurements. Results showed that Terra/MODIS VIs correlated to field data better than FY-3A/MERSI VIs, which was attributed to the broader FY-3A/MERSI bandwidth that are more sensitive to atmospheric influences. Ge et al. (2007) found strong correlation between FY-3A/MERSI and Terra/MODIS VIs (R = 0.99) and further confirmed the sensitivity of MERSI reflectance to atmospheric water vapor content based on MODTRAN simulation (especially when water vapor content was greater than $5g/cm^2$).

There are also several studies that utilized VI time series from CEOS sensors to study vegetation phenology(Li et al. 2017; Yang et al. 2017; Wang et al. 2014). For instance, Song et al. (2018) extracted phenological information for double-cropping rice using 30-m HJ-1/CCD data and results showed that sub-field rice growth can be reflected. Li et al. (2019) used same HJ-1/CCD data to study forest phenology and then analyzed how tree phenology responded to meteorological forcing.

3.2 Fractional Vegetation Cover

Fractional Vegetation Cover (FVC) is expressed as a percentage of the vertical projected area of vegetation (including stems, leaves, and branches) to the ground area (Gitelson et al. 2002), which is widely used in land degradation analysis and also an input to surface energy balance and hydrological models (Pettorelli et al. 2005b; Wang et al. 2020; Younes et al. 2019). Liu et al. (2019) performed FVC retrieval using GF-1/WFV and PMS based on the image dimidiate pixel method and found that the uncertainty of PMS was lower than WFV due to higher spatial resolution, resulting more details about spatial soil/vegetation heterogeneity that is beneficial for land degradation assessment. Sun et al. (2015) found that GF-1/WFV provided FVC retrievals of better accuracy than Landsat-8/OLI in sparse grassland ecosystems and further reported that correction of view angle effect resulted from large swath of GF-1/WFV and HJ-1/CCD NDVI can reduce the FVC retrieval uncertainty by 7.5% - 7.8% (Sun et al. 2020).

Zhang et al. (Zhang et al. 2013) retrieved FVC using VIs calculated from HJ-1/HSI hyperspectral data through an optimal band combination approach and found a good accuracy ($R^2 = 0.86$, RMSE = 0.11). Due to the high spatial resolution of HJ-1/HSI, Liao & Zhang (2020) was able to optimize the selection of endmember spectrum for theoretically pure vegetation, shaded, and soil based on Pixel Purity Index (PPI) and Endmember Average Root mean square error (EAR), and then retrieved FVC using the MESMA (Multiple Endmember Spectral Mixture Analysis) method. Results showed that with a good spatial resolution and high spectral resolution, the accuracy of the HJ-1/HSI FVC retrieval was high (RMSE = 0.19). Bian et al. (2017) proposed an adaptive endmember selection linear spectral mixture model (ASLSMM) based on HJ-1/CCD data to enhance the accuracy of FVC estimation and found that compared with the traditional LSMM and MESMA methods, the ASLSMM method is more representative of the ground truth, and the inversion results are efficient and accurate. Liu et al. (2021) applied FY-3B/MERSI data to estimate FVC using PROSAIL model and random forest method and the results showed good agreement with the EOLAB (Earth Observation Laboratory) reference FVC data (RMSE = 0.13).

3.3 Leaf Area Index

Leaf Area Index (LAI) refers to the total area of plant leaves per unit land area (Chen and Black 1992) and is a key determinant of net primary productivity of ecosystems and energy exchange between the atmosphere and land surface (Wang et al. 2019a; Yan et al. 2019). Li et al. (2016) used a statistical regression approach to estimate LAI in winter wheat cropland from HJ-1/CCD with good accuracy (RRMSE = 29.15%). Wei et al. (2017c) and Lei et al. (2018) applied the physical PROSAIL model to retrieve LAI from GF-1/WFV in maize crop and *Acacia Ricchii* plantation respectively and reported similar accuracies (RMSE = 0.5 m^2 for maize crop, and RMSE = 0.13 m^2 for *Acacia Ricchii* plantation).

In addition to empirical and physical model-based approach, machine learning (ML) has also been used to retrieve LAI from CEOS data. Lei et al. (2018) found ML-based approach offered higher accuracy (RMSE = 0.50 m^2) in estimating LAI than the empirical VI-based regression approach (RMSE = 0.67 m^2). Wei et al. (2017a) estimated LAI for cropland from GF-5/AHSI hyperspectral data using the RF-KNN model (RMSE = 0.70 m^2).

3.4 Aboveground Biomass

Aboveground Biomass (AGB) refers to the total amount of plant-derived living and dead organic matter per unit of surface area, which is an important component of terrestrial carbon cycle. Accurate estimation of the spatial and temporal AGB variations is critical to many application such as crop yields estimation, pasture forage and forest timber production (Brown et al. 1996; Lu 2006). Wang et al. (2014b) estimated the AGB of the Yellow River Estuary wetlands from GF-1/WFV using statistical regression approach (MRE (Mean Relative Error) = 23.9%). Gou et al. (2019) used VIs in conjunction with texture information extracted from GF-2/PMS high-resolution images to estimate the AGB of *Pinus tabuliformis* plantations and obtained a similar accuracy (RMSE = 0.43 t/hm^2). Gao et al. (2019) first retrieved AGB using high-resolution unmanned aerial vehicle (UAV) measurement and then scaled up to regional scale by establishing a regression model using GF-1/WFV NDVI, the uncertainty is RMSE = 68.04 g/m^2 , which is much smaller than using GF-1/WFV only with RMSE = 128.75 g/m^2 .

Gao et al. (2014) established the regression model between VIs acquired from ZY-3/MUX and ground measured shrub AGB in mountainous areas. Due to the capability for acquiring multi-angle observations with the three TDI cameras forming a camera array that can obtain stereo image, from which detailed topographic information can be used to improve AGB estimation by applying accurate topographic correction, leading to a reduction of SD (Standard Deviation) drop by 21.2%. Taking the advantage of the multitemporal high-resolution multispectral and stereo images taken by ZY-3/TDI, Li et al. (2019a) further proposed an improved workflow for estimating forest AGB based on the retrieval of relative canopy height, which led to a high accuracy in AGB estimation (RMSE = 24.49 Mg/ha, RRMSE =21.37%) compared with using spectral data only (RMSE = 33.89 Mg/ha, RRMSE = 29.57%).

4 Research opportunities offered by the addition of CEOS sensors

4.1 Multi-sensor data fusion

Observations from single satellite sensor often comprise spatial resolution for temporal resolution, or vice versa, resulted in sub-optimal monitoring of vegetation dynamics. Data fusion is an effective way for achieving both high spatial and temporal resolutions by fusing data from different sensors. Pi et al. (2021) reconstructed a NDVI dataset with 16 m spatial and 16-day temporal resolutions by fusing GF-1/WFV with MOD13Q1 NDVI based on the STARFM (Spatial and Temporal Adaptive Reflectance Fusion Model) algorithm. Yin et al. (2016) found that by fusing EOS/MODIS and FY-3/MERSI observations, which share high similarity in terms of spectral band configuration, the spatio-temporal gaps of LAI retrievals were significantly reduced, leading to more valid data over the cloud-prone sub-tropical and tropical forests. Wu et al. (2015) applied the Spatial and Temporal Data Fusion Approach (STDFA) to create a daily NDVI time series for crop phenology monitoring through the fusion of HJ-1/CCD or GF-1/WFV with MODIS, with the output revealed detailed sub-field crop growth at daily time-step.

4.2 Data continuity & data recovery

For global change studies, it is critical to ensure long-term data continuity and high-level or data consistency. China is launching and planning to launch many new spaceborne sensors covering a wide range of sensor types and spatial-temporal resolutions, offering great potentials to achieve sustainable monitoring of global change into the foreseeing future, or at least used as backup for other commonly used sensors. For instance, the CEOS GF-5/AHSI hyperspectral instrument with 30 m spatial resolution and 330 narrow spectral bands, in together with ASI/PRISMA and DLR/DESIS, can be good successors for the highly-successful EO-1/Hyperion which has ceased operation since 2014.

In other occasions, orbiting sensor can encounter instrument failure that if similar instruments are available from other satellite, a virtual constellation can be formed to mimic the functioning (He et al. 2018; Yueh et al. 2016). One example is the recovery of the SMAP mission after the radar failure by ingesting data from ESA's Sentinel-1 C-band SAR (Meyer et al. 2021), something that can also be done using GF-3 C-band SAR. Another example is filling the data gaps caused by the Scan-Line-Corrector (SLC) failure of Landsat-7/ETM+ using Sentinel-2/MSI (Wang et al. 2021), resulted in seamless imagery that greatly improved the related scientific applications. This type of effort might be further improved by using HJ-1/CCD started operating from 2009 that has same 30-m resolution and nearly identify spectral band configuration as ETM+ (Figure 3). These are all beneficial to the end users in global vegetation and ecological remote sensing community.

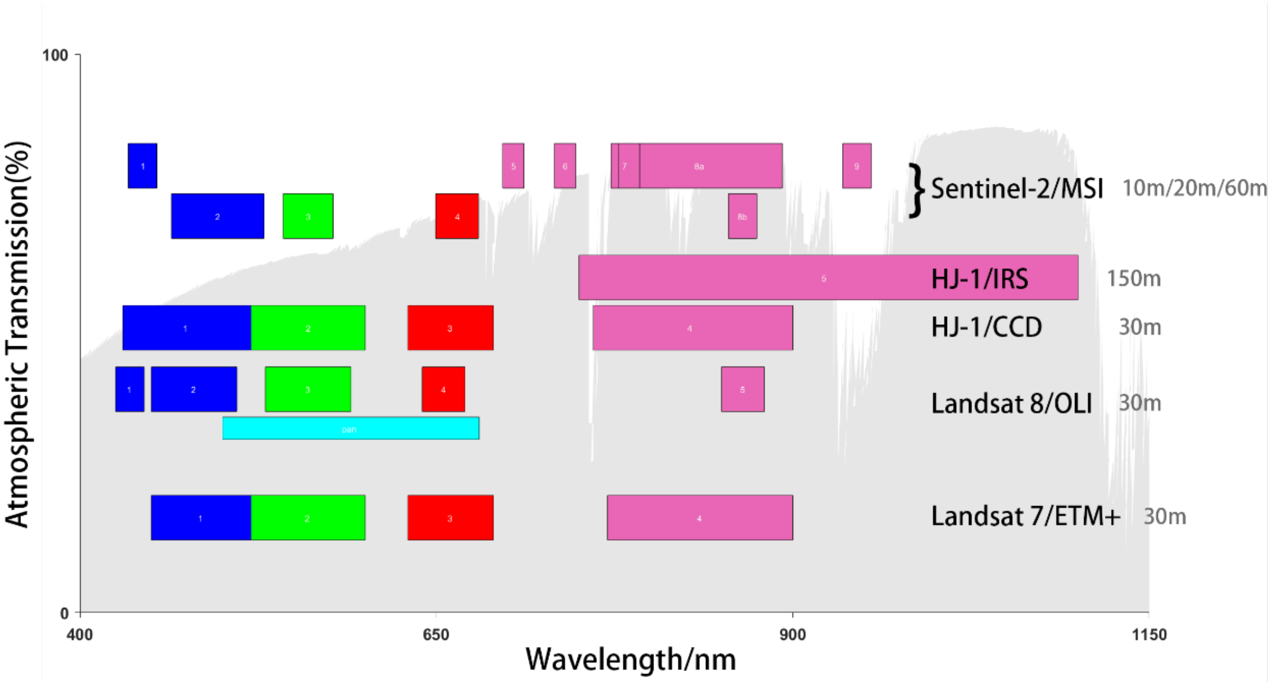

Figure 3 Spectral band comparisons among Landsat-7/ETM+, Landsat-8/OLI, HJ-1/CCD, HJ-1/IRS, and Sentinel-2/MSI.

4.3 Multi-angle remote sensing

Multi-angle remote sensing is an effective way to infer surface BRDF (Bidirectional Reflectance Distribution Function) that can be further used to retrieve albedo or estimate vegetation structure (Yan et al. 2021). BRDF retrieval using single-sensor data often suffers from the problem of limited angular sampling due to cloud or aerosols, e.g., MODIS has only a 75.8% probability that have more than 7 cloud-free observations within a 16 d window (Wen 2015). Multi-sensor data can be combined to accumulate a sufficient number of multi-angle observations in a shorter time for improved BRDF retrievals. In addition, multi-angle data can also be used to improve the retrievals of vegetation parameters. Bicheron et al. (1999) reported that forest classification uncertainty can be reduced if multi-spectral data is used in conjunction with multi-angle data that providing additional information about forest canopy structure (Hyman and Barnsley 1997). For instance, Wen et al. (2016) developed a multi-sensor combined BRDF inversion (MCBI) by ingesting data from MODIS, AVHRR, VIIRS and FY-3/MERSI, leading to a much shortened retrieval window up to 4 days in comparison to the standard 16-day window of using MODIS only.

5 Concluding remarks and future perspectives

It is therefore all about the benefit to the end-users in scientific community. Over past half century the scientific community has benefited enormously from the ever-improving open EO data policy, one example is the boost of research after the release of full Landsat archive (Wulder et al. 2012). The past decade has overseen immense amount of investment from China on EO missions, creating now a spaceship fleet encompassing a full-suite of sensors to some extent resembling the fleet from

NASA, ESA, JAXA and other major space agencies. More studies that attempting to use or integrate CEOS data are highly encouraged to not only gain experiences in using CEOS data for vegetation and ecological remote sensing. Meanwhile, and hence critically identify the pros and cons of these newly orbiting scientific instruments. Now most applications as we reviewed above are still from Chinese research community, therefore international users are also encouraged to access the data as most of the data we reviewed above are publicly available (with user registration sometimes required) and have data access webpage in English language. The valuable experiences and critics gain from both the domestic and international end-users would in turn be used to further improve all aspects of CEOS sensors and eventually lead to a better understanding of pressing scientific issues such global environmental change, sustainability development, food security and biodiversity conservation. While this article is being read, CEOS sensors are continuously measuring reflectance and echo over the entire planet. It is now the time to capitalize them for the benefit of global vegetation monitoring.

Acknowledgement

This study is supported by National Natural Science Foundation of China (No. 42171305, Principal Investigator: X. Ma); Natural Science Foundation of Gansu Province, China (No. 21JR7RA499, PI: X. Ma); Fundamental Research Funds for the Central Universities (No. lzujbky-2021-ct11, PI: X. Ma). We thank Yifei Gao for helping preparing the reference list.

Appendix

Table A1 Comparison between GF-1(6)/WFV and Sentinel-2/MSI

Satellite	Sensor	Band No.	Spectral Range (μm)	Spatial Resolution at nadir (m)	Swath Width (km)	Revisit Cycle (days)
GF-1	Wide-Field View Multispectral Camera (WFV)	1	0.45~0.52	16	800 (with 4 Cameras)	2
		2	0.52~0.59			
		3	0.63~0.69			
		4	0.77~0.89			
GF-6		1	0.45~0.52	16		
		2	0.52~0.59			
		3	0.63~0.69			
		4	0.77~0.89			
		5	0.69~0.73			
		6	0.73~0.77			
		7	0.40~0.45			
		8	0.59~0.63			
Sentinel -2	Multi-Spectral Instrument (MSI)	2	0.458~0.523	10	290	5
		3	0.543~0.578			
		4	0.65~0.68			
		8	0.785~0.90			
		5	0.698~0.713	20		
		6	0.733~0.748			
		7	0.773~0.793			
		8A	0.855~0.875			
		11	1.565~1.655			
		12	2.10~2.28			
		1	0.433~0.453	60		
		9	0.935~0.955			
		10	1.365~1.385			

Table A2 Comparison between GF-1(6)/PMS, ZY-3/MUX and SPOT-6(7)/NAOMI

Satellite	Sensor	Band No.	Spectral Range (μm)	Spatial Resolution at nadir (m)	Swath Width (km)	Revisit Cycle (days)
GF-1/6	Panchromatic & Multispectral Camera (PMS)	pan	0.45~0.90	2	60 (with 2 Cameras)	4
		1	0.45~0.52	8		
		2	0.52~0.59			
		3	0.63~0.69			
		4	0.77~0.89			
ZY-3	Multispectral Camera (MUX)	1	0.45~0.52	6	51	5
		2	0.52~0.59			
		3	0.63~0.69			
		4	0.77~0.89			
SPOT-6/7	New Astrosat Optical Modular Instrument (NAOMI)	pan	0.45~0.75	1.5	60	1 (with 2 Cameras)
		1	0.45~0.52	6		
		2	0.53~0.6			
		3	0.62~0.69			
		4	0.76~0.89			

Table A3 Comparison between GF-2/PMS and WorldView-3/WV110

Satellite	Sensor	Band No.	Spectral Range (μm)	Spatial Resolution at nadir (m)	Swath Width (km)	Revisit Cycle (days)
GF-2	Panchromatic & Multispectral Camera (PMS)	pan	0.45~0.90	1	45(with 2 Cameras)	5
		1	0.45~0.52	4		
		2	0.52~0.59			
		3	0.63~0.69			
		4	0.77~0.89			
WorldView-3	WorldView-110 camera (WV110)	pan	0.45-0.80	0.31	13.1	1(4.5) day(s) at 1(0.59)-meter GSD resolution
		1	0.40~0.45	1.24		
		2	0.45~0.51			
		3	0.51~0.58			
		4	0.585~0.625			
		5	0.63~0.69			

	6	0.705~0.745	
	7	0.77~0.895	
	8	0.86~1.04	
	SWIR	1.195~2.365	3.7
	CAVIS	0.405~2.245	30

Table A4 Comparison of SAR satellites between GF-3 and Sentinel-1

Satellite	Sensor	Operational Mode	Spatial Resolution at nadir (m)	Swath Width (km)	Polarization Mode(Selectable)
GF-3	C-band Synthetic Aperture Radar (SAR)	SL	1	10	single-polarization
		UFS	3	30	single-polarization
		FS1	5	50	dual-polarization
		FS2	10	100	dual-polarization
		SS	25	130	dual-polarization
		NSC	50	300	dual-polarization
		WSC	100	500	dual-polarization
		QPS1	8	30	full polarization
		QPS2	25	40	full polarization
		WAVE	10	5	full polarization
		GLOGAL	500	650	dual-polarization
		EXTENDED1	25	130	dual-polarization
		EXTENDED2	25	80	dual-polarization
Sentinel-1	C-band Synthetic Aperture Radar (SAR)	SM	5	80	full polarization
		IW	5×20	250	full polarization
		EW	25×100	400	full polarization
		WV	5×20	20	single-polarization

Table A5 Comparison of Hyperspectral satellites between GF-5/AHSI, HJ-1A/HIS, DLR/DESIS and PRISM

Satellite	Sensor	Number of Bands	Spectral Range (μm)	Spectral Resolution(nm)	Spatial Resolution at nadir (m)	Swath Width (km)	Revisit Cycle (days)
HJ-1A	Hyperspectral Imager (HSI)	110-128	0.45~0.95	3.9~4.5	100	50	4
GF-5	Advanced Hyperspectral Imager (AHSI)	300	0.40~2.50	5(VNIR) 10(SWIR)	30	60	5
DLR	DLR Earth Sensing Imaging Spectrometer (DESIS)	235	0.40~1.00	2.55	30	30	3-5
PRISMA	-	240	0.40~2.50	< 12	30	30	7

References

Aplin, P. (2005). Remote sensing：ecology. Progress in Physical Geography, 104-113

Bannari, A., Morin, D., Bonn, F., & Huete, A. (1995). A review of vegetation indices. Remote sensing reviews, 13, 95-120

Bian, J.H., Li, A.N., Zhang, Z.J., Zhao, W., Lei, G.B., Yin, G.F., Jin, H.A., Tan, J.B., & Huang, C.Q. (2017). Monitoring fractional green vegetation cover dynamics over a seasonally inundated alpine wetland using dense time series HJ-1A/B constellation images and an adaptive endmember selection LSMM model. Remote Sensing of Environment, 197, 98-114

Bicheron, P., & Marc, L. (1999). A method of biophysical parameter retrieval at global scale by inversion of a vegetation reflectance model. Remote Sensing of Environment, 1999, 251-266

Brown, S., Sathaye, J.A., & Kauppi, P. (1996). Mitigation of carbon emissions to the atmosphere by forest management. Commonwealth Forestry Review

Chen, J.M., & Black, T.A. (1992). Defining Leaf-Area Index for Non-Flat Leaves. Plant Cell and Environment, 15, 421-429

Chen, X., & Liu, Z. (2015). Quantitative Analysis of Relationship Between HJ-1NDVI and MODIS NDVI. Remote Sensing Information

Cohen, W.B., & Goward, S.N. (2004). Landsat's role in ecological applications of remote sensing. BioScience, 54, 535-545

Davis, C.L., Hoffman, M.T., & Roberts, W. (2017). Long-term trends in vegetation phenology and productivity over Namaqualand using the GIMMS AVHRR NDVI3g data from 1982 to 2011. South African Journal of Botany, 111, 76-85

Dong, C.H., Yang, J., Zhang, W.J., Yang, Z.D., Lu, N.M., Shi, J.M., Zhang, P., Liu, Y.J., & Cai, B. (2009). An Overview of a New Chinese Weather Satellite FY-3A. Bulletin of the American Meteorological Society, 90, 1531-+

Feng, L., Guo, S., Zhu, L.J., Fang, X.Q., & Zhou, Y.A. (2017). Urban vegetation phenology analysis and the response to the temperature change. 2017 Ieee International Geoscience and Remote Sensing Symposium (Igarss), 5743-5746

Gao, M.L., Zhao, W.J., Gong, Z.N., Gong, H.L., Chen, Z., & Tang, X.M. (2014). Topographic Correction of ZY-3 Satellite Images and Its Effects on Estimation of Shrub Leaf Biomass in Mountainous Areas. Remote Sensing, 6, 2745-2764

Gao, Y., Liang, Z., Wang, B., Wu, Y., & Liu, S. (2019). UAV and satellite remote sensing images based aboveground biomass inversion in the meadows of Lake Shengjin. Journal of Lake Sciences, 31, 517-528

Ge, M., Zhao, J., Zhong, B., & Yang, A. (2017). Comparison of the Vegetation Indexes between FY-3/VIRR,FY-3/MERSI and EOS/MODIS Data. Remote Sensing Technology and Application, 32, 12

Gianelle, D., Vescovo, L., & Mason, F. (2009). Estimation of grassland biophysical parameters using hyperspectral reflectance for fire risk map prediction. International journal of wildland fire, 18, 815-824

Gitelson, A.A., Kaufman, Y.J., Stark, R., & Rundquist, D. (2002). Novel algorithms for remote estimation of vegetation fraction. Remote Sensing of Environment, 80, 76-87

Gou, R., Chen, J., Duan, G., Yang, R., Bu, Y., Zhao, J., & Zhao, P. (2019). Inversion of aboveground biomass of Pinus tabuliformis plantations based on GF-2 data. Chinese Journal of Applied Ecology, 30, 4031-4040

He, L., Hong, Y., Wu, X., Ye, N., Walker, J.P., & Chen, X. (2018). Investigation of SMAP Active–Passive Downscaling Algorithms Using Combined Sentinel-1 SAR and SMAP Radiometer Data. IEEE Transactions on Geoscience and Remote Sensing, 56, 4906-4918

Huang, W., Sun, S.R., Jiang, H.B., Gao, C., & Zong, X.Y. (2018). GF-2 Satellite 1m/4m Camera Design and In-Orbit Commissioning. Chinese Journal of Electronics, 27, 1316-1321

Hyman, A.H., & Barnsley, M.J. (1997). On the potential for land cover mapping from multiple-view-angle (MVA) remotely-sensed images. International Journal of Remote Sensing, 18, 2471-2475

Kalaitzidis, C., Heinzel, V., & Zianis, D. (2010). A review of multispectral vegetation indices for biomass estimation. In, Proceedings of the 29th symposium of the European association of remote sensing laboratories, Chania, Greece. IOS Press Ebook (pp. 201-208)

Kerr, J.T., & Ostrovsky, M. (2003). From space to species: ecological applications for remote sensing. Trends in Ecology & Evolution, 18, 299-305

Lei, Y., Zhu, S., Guo, Y., Li, D., Liu, L., & Liu, N. (2018). Inversion of Leaf Area Index Based on Extreme Learning Machine Regression in Road Vegetation. Bulletin of Surveying and Mapping, 5

Li, D. (2012). China's First Civilian Three-line-array Stereo Mapping Satellite: ZY-3 Acta Geodaetica et Cartographica Sinica, 41, 317-322

Li, G.Y., Xie, Z.L., Jiang, X.D., Lu, D.S., & Chen, E.X. (2019a). Integration of ZiYuan-3 Multispectral and Stereo Data for Modeling Aboveground Biomass of Larch Plantations in North China. Remote Sensing, 11

Li, H., Chen, Z.X., Jiang, Z.W., Wu, W.B., Ren, J.Q., Liu, B., & Hasi, T. (2017). Comparative analysis of GF-1, HJ-1, and Landsat-8 data for estimating the leaf area index of winter wheat. Journal of Integrative Agriculture, 16, 266-285

Li, H., Peng, R., Li, W., Zhu, X., Huang, Y., & Nie, Q. (2019 b). Filtering algorithms of HJ-1 A/B NDVI time series data and phenology of typical tree species in Xiamen. Chinese Journal of Ecology

Li, X., Zhang, Y., Luo, J., Jin, X., Xu, Y., & Yang, W. (2016). Quantification winter wheat LAI with HJ-1CCD image features over multiple growing seasons. International Journal of Applied Earth Observation and Geoinformation, 44, 104-112

Li, F., Song, G., Liujun, Z., Xiuqin, F., & Yanan, Z. (2017). Urban vegetation phenology analysis and the response to the temperature change. In, 2017 IEEE International Geoscience and Remote Sensing Symposium (IGARSS) (pp. 5743-5746): IEEE

Liu, D.Y., Jia, K., Jiang, H.Y., Xia, M., Tao, G.F., Wang, B., Chen, Z.L., Yuan, B., & Li, J. (2021). Fractional Vegetation Cover Estimation Algorithm for FY-3B Reflectance Data Based on Random Forest Regression Method. Remote Sensing, 13

Liu, R., Ren, H., Liu, S., Liu, Q., Yan, B., & Gan, F. (2018). Generalized FPAR estimation methods from various satellite sensors and validation. Agricultural and Forest Meteorology, 260, 55-72

Liu, Z., Mo, R., Sun, X., & Lv, X. (2019). Analysis of Influence of GFn-1 Data Resolution on Extraction of Vegetation Coverage Information. Rural Economy and Science-Technology, 30, 80-82

Lu, D. (2006). The potential and challenge of remote sensing-based biomass estimation. International Journal of Remote Sensing, 27, 1297-1328

Mancino, G., Ferrara, A., Padula, A., & Nolè, A. (2020). Cross-Comparison between Landsat 8 (OLI) and Landsat 7 (ETM+) Derived Vegetation Indices in a Mediterranean Environment. Remote Sensing, 12

Meyer R, Zhang W, Kragh S J, et al. Exploring the combined use of SMAP and Sentinel-1 data for downscaling soil moisture beyond the 1 km scale[J]. Hydrology and Earth System Sciences Discussions, 2021: 1-25.

Nara, H., & Sawada, Y. (2021). Global Change in Terrestrial Ecosystem Detected by Fusion of Microwave and Optical Satellite Observations. Remote Sensing, 13

Pan, T. (2015). Technical Characteristics of GF-2 Satellite. Aerospace China, 3-9

Pettorelli, N. (2013). The normalized difference vegetation index. Oxford University Press

Pettorelli, N., Vik, J.O., Mysterud, A., Gaillard, J.-M., Tucker, C.J., & Stenseth, N.C. (2005). Using the satellite-derived NDVI to assess ecological responses to environmental change. Trends in ecology & evolution, 20, 503-510

Pi, X., Zeng, Y., & He, C. (2021). Estimating urban vegetation coverage on the basis of multi-source remote sensing data and temporal mixture analysis. Journal of Remote Sensing, 25, 1216-1226

Song, D., Wang, Z., Li, Y., & Hu, Y. (2018). Cropland Phenology Detection Based on HJ-1A/B CCD Data in Jianghan Plain. Geomatics & Spatial Information Technology, 41, 5

Sun, Z., Liu, S., Jiang, J., Bai, X., Chen, Y., Zhu, C., & Guo, W. (2017). Coordination inversion methods for vegetation cover of winter wheat by multi-source satellite images. Transactions of the Chinese Society of Agricultural Engineering, 33, 7

Tang, X., & Hu, F. (2018). Development Status and Trend of Satellite Mapping. Spacecraft Recovery & Remote Sensing, 39, 26-35

Wang, J., Li, X., & Fan, W. (2014a). Monitoring Vegetation Phenology Using HJ-CCD Image of High and Moderate Resolution Remote Sensing Data:A Case Study in Upper Stream of Miyun Reservoir. Journal of Northeast Forestry University, 88-94

Wang, J., Zhang, J., Ma, Y., & Ren, G. (2014b). Study on the Above Ground Vegetation Biomass Estimation Model Based on GF-1 WFV Satellite Image in the Yellow River Estuary Wetland. Acta Laser Biology Sinica, 604-608

Wang, Q., Wang, L., Wei, C., Jin, Y., Li, Z., Tong, X., & Atkinson, P.M. (2021). Filling gaps in Landsat ETM+ SLC-off images with Sentinel-2 MSI images. International Journal of Applied Earth Observation and Geoinformation, 101

Wang, S., Zhang, B., Zhai, X., & Sun, H.-l. (2020). Vegetation cover changes and sand-fixing service responses in the Beijing–Tianjin sandstorm source control project area. Environmental Development, 34, 100455

Wang, Y.C., Liu, Y.X., Li, M.C., & Tan, L. (2014). The reconstruction of abnormal segments in HJ-1A/B NDVI time series using MODIS: a statistical method. International Journal of Remote Sensing, 35, 7991-8007

Wang, Z.Z., Li, J.Y., He, J.Y., Zhang, S.W., Gu, S.Y., Li, Y., Guo, Y., & He, B.Y. (2019). Performance Analysis of Microwave Humidity and Temperature Sounder Onboard the FY-3D Satellite From Prelaunch Multiangle Calibration Data in Thermal/Vacuum Test. IEEE Transactions on Geoscience and Remote Sensing, 57, 1664-1683

Wei, X., Gu, X., Meng, Q., Yu, T., Zhou, X., Wei, Z., Jia, K., & Wang, C. (2017a). Leaf Area Index Estimation Using Chinese GF-1 Wide Field View Data in an Agriculture Region. Sensors (Basel), 17

Wei, X.Q., Gu, X.F., Meng, Q.Y., Yu, T., Jia, K., Zhan, Y.L., & Wang, C.M. (2017b). Cross-Comparative Analysis of GF-1 Wide Field View and Landsat-7 Enhanced Thematic Mapper Plus Data. Journal of Applied Spectroscopy, 84, 829-836

Wei, X.Q., Gu, X.F., Meng, Q.Y., Yu, T., Zhou, X., Wei, Z., Jia, K., & Wang, C.M. (2017c). Leaf Area Index Estimation Using Chinese GF-1 Wide Field View Data in an Agriculture Region. Sensors, 17

Wen, J. (2015). Remote Sensing Modeling and Albedo Inversion of Land Surface Bidirectional Reflectance Characteristics. Science Press

Wen J, Dou B, You D, et al. Forward a small-timescale BRDF/Albedo by multisensor combined brdf inversion model[J]. IEEE Transactions on Geoscience and Remote Sensing, 2016, 55(2): 683-697.

Wu, M.Q., Zhang, X.Y., Huang, W.J., Niu, Z., Wang, C.Y., Li, W., & Hao, P.Y. (2015). Reconstruction of Daily 30 m Data from HJ CCD, GF-1 WFV, Landsat, and MODIS Data for Crop Monitoring. Remote Sensing, 7, 16293-16314

Wu, P., Hu, L., Li, G., Feng, Z., & Chen, C. (2011). Relationship between FY-3A/MERSI and MODIS Vegetation Indexes Based on Cotton Spectrum. Desert and Oasis Meteorology, 5, 4

Wulder, M.A., Hall, R.J., Coops, N.C., & Franklin, S.E. (2004). High spatial resolution remotely sensed data for ecosystem characterization. BioScience, 54, 511-521

Yan, G., Hu, R., Luo, J., Weiss, M., Jiang, H., Mu, X., Xie, D., & Zhang, W. (2019). Review of indirect optical measurements of leaf area index: Recent advances, challenges, and perspectives. Agricultural and Forest Meteorology, 265, 390-411

Yan, G., Jiang, H., Yan, K., Cheng, S., Song, W., Tong, Y., Liu, Y., Qi, J., Mu, X., Zhang, W., Xie, D., & zhou, H. (2021). Review of optical multi-angle quantitative remote sensing. National Remote Sensing Bulletin, 25, 83-108

Yang, Z., Shao, Y., Li, K., Liu, Q., Liu, L., & Brisco, B. (2017). An improved scheme for rice phenology estimation based on time-series multispectral HJ-1A/B and polarimetric RADARSAT-2 data. Remote Sensing of Environment, 195, 184-201

Yin, G., Li, J., Liu, Q., Zhong, B., & Li, A. (2016). Improving LAI spatio-temporal continuity using a combination of MODIS and MERSI data. Remote Sensing Letters, 7, 771-780

Younes, N., Joyce, K.E., Northfield, T.D., & Maier, S.W. (2019). The effects of water depth on estimating Fractional Vegetation Cover in mangrove forests. International Journal of Applied Earth Observation and Geoinformation, 83

Yuan, Z., Yang, A., & Zhong, B. (2015). Cross comparison of the vegetation indexes between Landsat TM and HJ CCD. Remote Sensing for Land & Resources, 27, 5

Yueh, S., Entekhabi, D., O'Neill, P., Njoku, E., & Entin, J. (2016). NASA soil moisture active passive mission status and science performance. 2016 IEEE International Geoscience and Remote Sensing Symposium (IGARSS)

Zhang, X., Zhou, M., Wang, W., & Li, X. (2015). Progress of global satellite remote sensing of atmospheric compositions and its' applications. Science & Technology Review, 33, 13-22

Zhang, X.F., Liao, C.H., Li, J., & Sun, Q. (2013). Fractional vegetation cover estimation in arid and semi-arid environments using HJ-1 satellite hyperspectral data. International Journal of Applied Earth Observation and Geoinformation, 21, 506-512

Zhang, Y., Song, C., Band, L.E., Sun, G., & Li, J. (2017). Reanalysis of global terrestrial vegetation trends from MODIS products: Browning or greening? Remote Sensing of Environment, 191, 145-155

Zhao, B., Wang, H., & Zhang, A. (2019). Inter-sensor comparison and quantitative relationships between GF-1 WFV and Landsat 8 OLI NDVI data. Journal of Geomatics, 44, 6

Zhao, J., Li, J., Liu, Q., Wang, H., Chen, C., Xu, B., & Wu, S. (2018). Comparative Analysis of Chinese HJ-1 CCD, GF-1 WFV and ZY-3 MUX Sensor Data for Leaf Area Index Estimations for Maize. Remote Sensing, 10

Zhao, K., Xu, J., Zhao, Z., Song, L., & Xiao, K. (2013). Cross Comparison of HJ-1A/B CCD and Landsat TM/ETM+ Multispectral Measurements for NDVI, SAVI and EVI Vegetation Index. Remote Sensing Technology and Application, 28, 8

Zhao, L., Zhang, R., Liu, Y., & Zhu, X. (2020). The differences between extracting vegetation information from GF1-WFV and Landsat8-OLI. Acta Ecologica Sinica, 40, 12

Zhou, X., Yamaguchi, Y., & Arjasakusuma, S. (2018). Distinguishing the vegetation dynamics induced by anthropogenic factors using vegetation optical depth and AVHRR NDVI: A cross-border study on the Mongolian Plateau. Sci Total Environ, 616-617, 730-743

Zoungrana, B.J.B., Conrad, C., Thiel, M., Amekudzi, L.K., & Da, E.D. (2018). MODIS NDVI trends and fractional land cover change for improved assessments of vegetation degradation in Burkina Faso, West Africa. Journal of Arid Environments, 153, 66-75

Rahman, A. F., Sims, D. A., Cordove, V. D., El-Marsri, B. Z. (2005). Potential of MODIS EVI and surface temperature for directly estimating per-pixel ecosystem C fluxes. Geophysical Research Letters, 32(19), L19404.